

Supporting Information

Low-Temperature-Grown p–n ZnO Nanojunction Arrays as Rapid and Self-Driven UV Photodetectors

Ming-Yen Lu^{a,*}, Hung-Yi Chen^b, Cheng-Yu Tsai^b, Yen-Ti Tseng^b, Yu-Ting Kuo^c, Hsiang-Chen Wang^b, and Ming-Pei Lu^d

^a Department of Materials Science and Engineering, National Tsing Hua University, Hsinchu 300, Taiwan

^b Graduate Institute of Opto-Mechatronics and ^c Department of Physics, National Chung Cheng University, Chia-Yi 62102, Taiwan

^d National Nano Device Laboratories, Hsinchu 300, Taiwan

- Hydrothermal growth of n- and p-ZnO NR arrays

20 mM Zinc acetate [$\text{Zn}(\text{CH}_3\text{COO})_2$] in ethanol was spun onto the substrate, which was then baked at 350 °C for 30 min to form the ZnO seed layer on the substrate. The undoped ZnO NR arrays were grown by immersing the seeded substrate into a growth solution of 25 mM zinc nitrate [$\text{Zn}(\text{NO}_3)_2$], 12.5 mM hexamethylenetetramine (HMTA), 5 mM polyethyleneimine (PEI; $M_w = 800$), and 0.8 M ammonium hydroxide (NH_4OH). PEI, a nonpolar polymer, was employed to suppress homogeneous nucleation in the growth solution, allowing formation of high-aspect-ratio ZnO NR arrays^{1, 2}. For p-ZnO NR array growth, antimony acetate [$\text{Sb}(\text{CH}_3\text{COO})_3$] was used as the dopant source. An equimolar mixture of sodium hydroxide (NaOH) and glycolic acid ($\text{C}_2\text{H}_4\text{O}_3$) in DI water was treated with $\text{Sb}(\text{CH}_3\text{COO})_3$ (to give a molar ratio of 1:12 to $\text{C}_2\text{H}_4\text{O}_3$) to form the Sb doping solution³. Various concentrations (0.05, 0.1, 0.2, and 0.4 mM) of the Sb doping solution were added into the growth solution to grow different p-ZnO NR arrays. Both the undoped and Sb-doped ZnO NR arrays were synthesized at 95 °C for 6 h. The Sb-doped ZnO NW arrays were then annealed at 850 °C for 30 min in the ambient atmosphere to activate the p-type dopants.

- p-n ZnO NR devices fabrication

The p–n ZnO nanojunctions were formed through two-step sequential growth: n-ZnO NR array growth (Figs. S1a and S1b) followed by selective p-ZnO NR array growth (Fig. S1c). To fabricate p–n ZnO nanojunction devices on a large scale, 200 nm Al was

deposited onto the n-ZnO NR arrays after the growth of the p–n ZnO nanojunction arrays (Fig. S1d). To avoid Ni metal from depositing on the bottom of the n-ZnO NRs in the p–n ZnO nanojunction region, the samples were spin-coated with methyl methacrylate (MMA), which was then etched with an oxygen plasma etcher until the p-ZnO NRs rose from the MMA surface (Fig. S1e). Ni was deposited on the p-ZnO NRs as the contact electrode (Fig. S1f). Finally, the MMA was removed by immersing the sample in acetone (Fig. S1g).

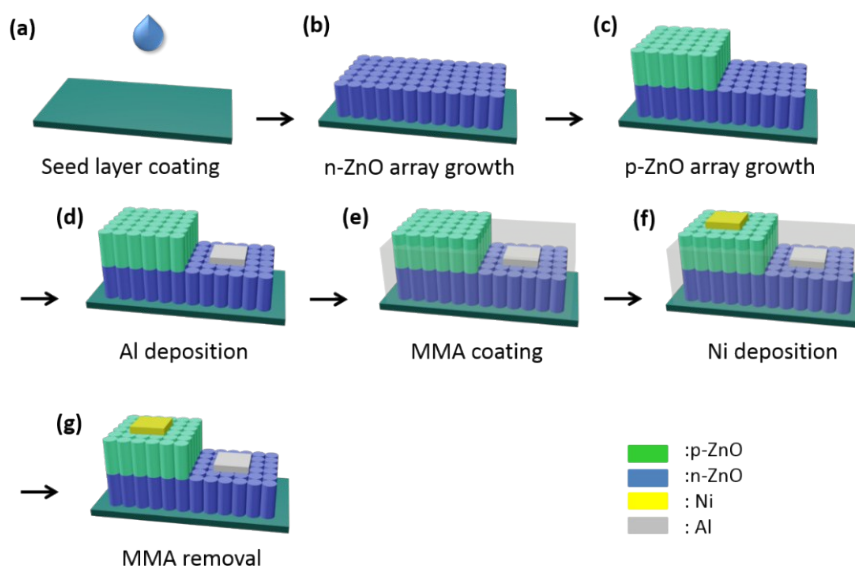


Fig. S1 Schematic representation of the device fabrication process.

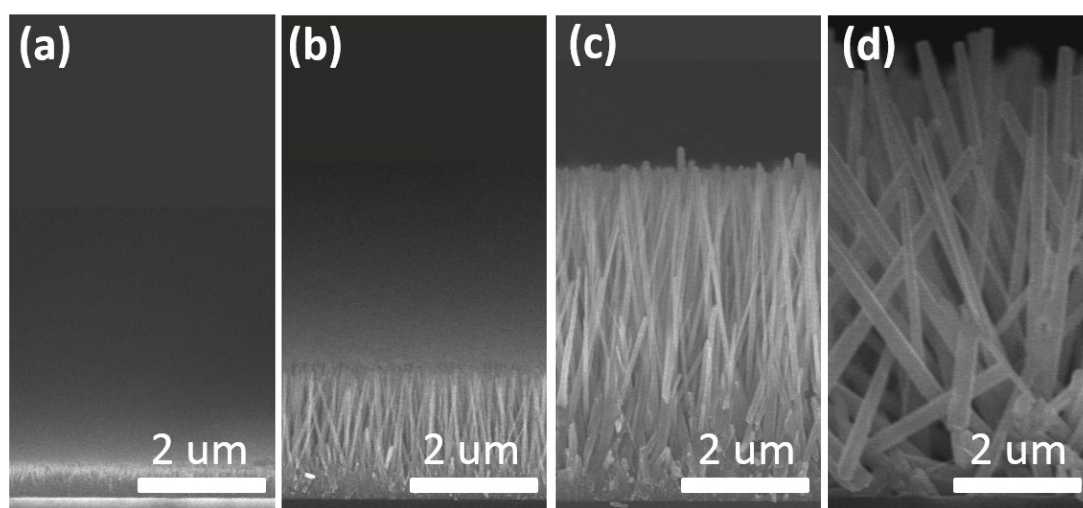


Fig. S2 Cross-sectional SEM images of undoped ZnO NR arrays grown using (a) 0.2, (b) 0.4, (c) 0.8, and (d) 1 M NH₄OH.

Photoluminescence Measurements

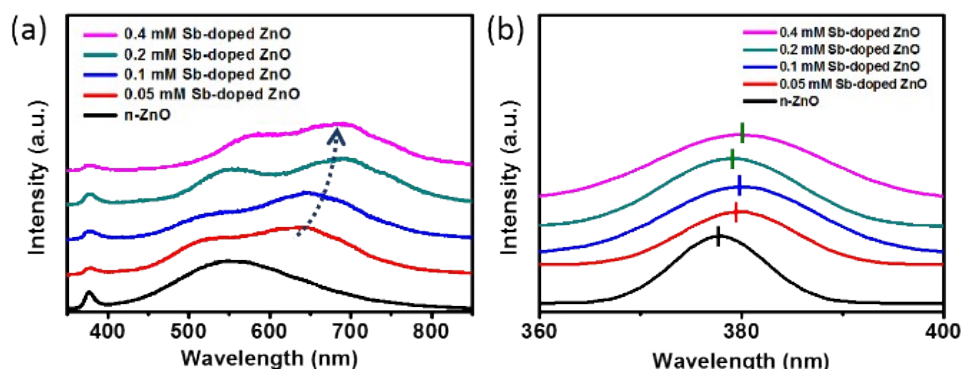


Fig. S3 (a) Room-temperature PL spectra of undoped and 0.05-, 0.1-, 0.2-, and 0.4-mM Sb-doped ZnO NR arrays. In addition to the UV- and oxygen-vacancy-related green emissions, a significant emission emerged in the visible range and shifted from 638 to 693 nm upon increasing the doping concentration. This emission, which has not been reported previously in the literature, may be due to radioactive recombination of electrons in $(\text{Sb}_{\text{Zn}}-2\text{V}_{\text{Zn}})$ complexes⁴. (b) Expanded view of the PL spectra displaying the near-band-edge emissions of the samples. The near-band-edge emission of Sb-doped ZnO NR arrays was red-shifted; this behavior has been observed previously and may be due to recombination of free excitons in Sb-doped ZnO NR arrays^{5,6}.

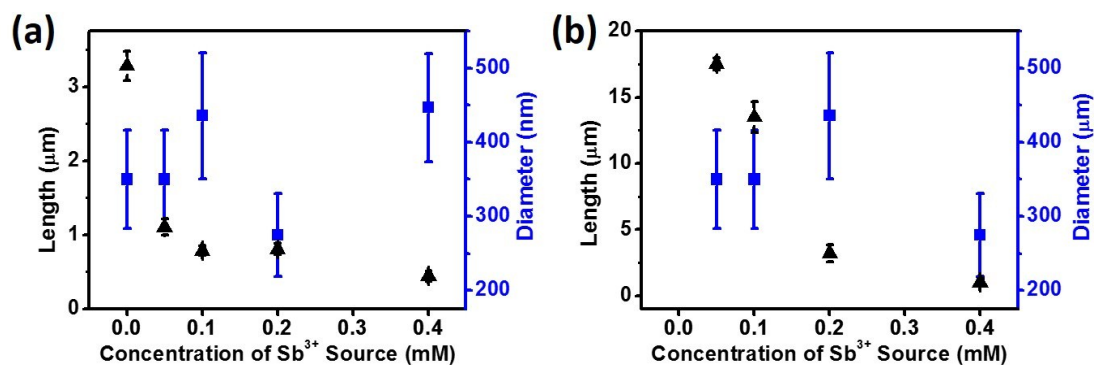


Fig. S4 Plots of the average lengths and diameters of Sb-doped ZnO NR arrays grown (a) on seeded substrates and (b) on undoped ZnO NR arrays. The lengths of the NRs grown on these two substrates displayed large differences, while their diameters were similar.

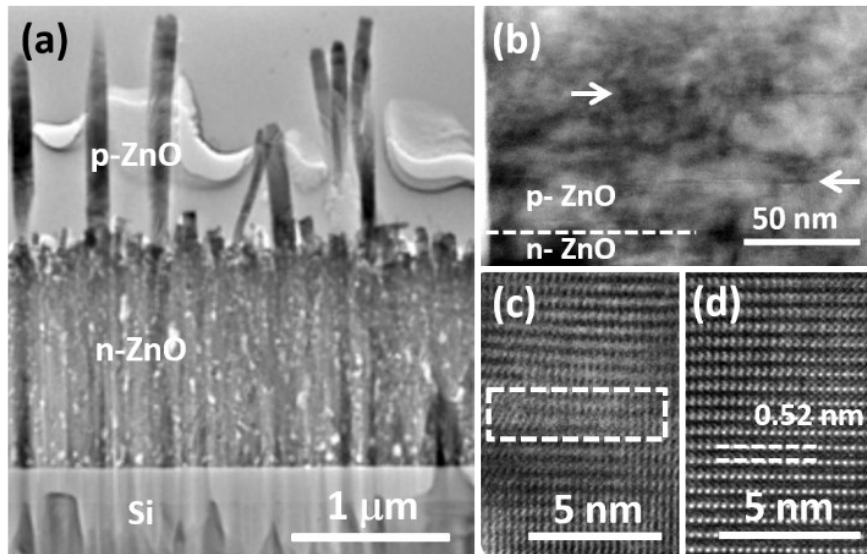


Fig. S5 (a) Low-magnification cross-sectional TEM image of a p-n ZnO nanojunction. (b) Magnified TEM image of the interface of the p-n ZnO nanojunction; stacking faults are found in the Sb-doped ZnO NRs. (c, d) High-resolution TEM images of the (c) Sb-doped and (d) undoped ZnO NRs. The lattice spacing of 0.52 nm corresponds to the (0001) plane of ZnO; the marked rectangle in (c) indicates the stacking fault.

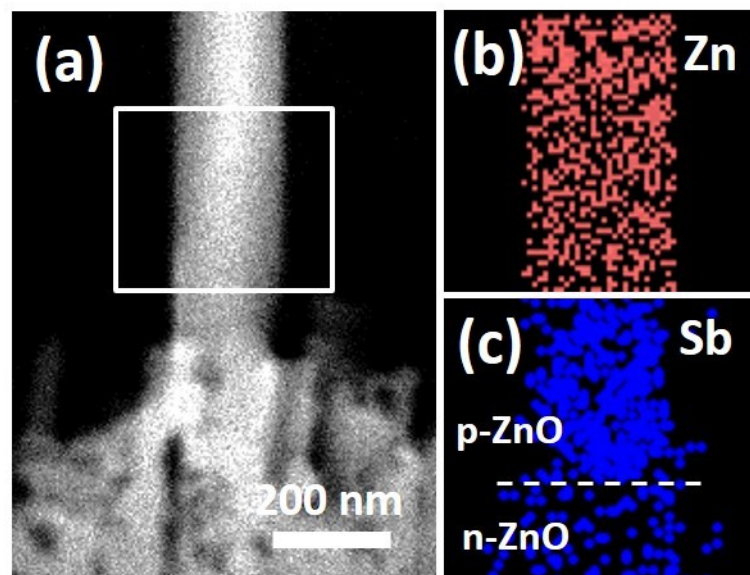


Fig. S6 (a) Scanning transmission electron microscopy image of a p-n ZnO NR. (b, c) Elemental mappings of (b) Zn and (c) Sb from the marked area in (a). The Sb elemental signals were densely distributed in the upper part of the NR, implying that the p-ZnO NR had grown directly on top of the n-ZnO NR.

References

1. C. K. Xu, P. Shin, L. L. Cao and D. Gao, *J. Phys. Chem. C*, 2010, **114**, 125-129.
2. M. Y. Lu, C. Y. Tsai, H. A. Chen, Y. T. Liang, K. P. Chen, S. Gradecak, S. Gwo and L. J. Chen, *Nano Energy*, 2016, **20**, 264-271.
3. X. D. Wang, F. W. Wang, F., J. H. Seo, D. Bayerl, J. A. Shi, H. Y. Mi, Z. Q. Ma, D. Y. Zhao, Y. C. Shuai and W. D. Zhou, *Nanotechnology*, 2011, **22**, 225602.
4. B. Xiang, P. W. Wang, X. Z. Zhang, S. A. Dayeh, D. P. R. Aplin, C. Soci, D. P. Yu and D. L. Wang, *Nano Lett.*, 2007, **7**, 323-328.
5. W. Dai, X. H. Pan, S. S. Chen, C. Chen, W. Chen, H. H. Zhang and Z. Z. Ye, *RSC Adv.*, 2015, **5**, 6311-6314.
6. T. H. Kao, J. Y. Chen, C. H. Chiu, C. W. Huang and W. W. Wu, *Appl Phys Lett*, 2014, **104**, 111909.